Research Paper

Struct Multidisc Optim 28, 127–135 (2004)
DOI 10.1007/s00158-003-0311-x

Why the grain in tree trunks spirals: a mechanical perspective

S. Leelavanichkul and A. Cherkaev

Abstract The trunks of Ponderosa pine are curiously designed: their grain spirals around the trunk. The natural question arises: why does the evolution lead to such complication in the design? Here, we attempt to find the answer considering the morphology of a trunk as a result of the optimization of a mechanical construction. We model the trunk as an anisotropic cylinder with helicoidal symmetry, compute the stresses, and optimize the angle of the grain's inclination using a strength criterion. When the structure of the tree is optimized only for the strength, the objective remains practically neutral to the variation of the angle of spiraling if the angle does not exceed a limit, then the strength declines. The measured angle in the Ponderosa pine corresponds to this limit. Another biological factor must be considered: the transportation of the fluid from the roots to the branches. The spiraling is needed to achieve the uniform watering of the branches across the trunk even if the roots grow from one side only. The analysis of the stresses in the anisotropic cylinder with helicoidal symmetry under bending and compression loads is performed by introducing elastic potentials which generalize the potentials for cylindrical anisotropy.

Key words spiral grain, anisotropic elasticity, wood failure, biomimetics

1 Introduction

The paper is concerned with the morphology of a tree's trunk from a structural optimization viewpoint. Specifically, we investigate reasons behind spiral groths of Ponderosa Pine trunks in southern Utah. These trees develop helicoidal wood fibers that wiggle around the trunk as spirals. Spiral grain can be seen on many trees; they are visible when the bark is removed from the trunk; the angle is about 30°–50°. The question is why do they twist. (Fig. 1).

Fig. 1 Ponderosa pine (photo by Cherkaev)

Many different reasons and hypotheses have been suggested to explain the spiraling, among them are such exotic factors as the earths rotation, the wind, and even the gravitational effect of the moon (Gedney 1986). The theory worked out by Kubler (1991) provides a convincing qualitative reason for the spiraling. A tree's branches with straight grain are fed only by those roots directly below them. If the roots on either side of the tree are cut, then branches on that side will die when the grain is straight. In contrast, each root of a spiraling grain tree feeds nearly the whole tree. If all the roots on one side die, that side of the tree will still be healthy. This has been proven (Kubler 1991) by injecting conifers with dye at the base. In addition to this consideration, trees become

Received: 4 June 2003
Revised manuscript received: 20 July 2004
Published online: 17 August 2004

S. Leelavanichkul and A. Cherkaev✉

Department of Mathematics, University of Utah, Salt Lake City, UT 84112, USA
e-mail: cherk@math.utah.edu

less stiff and bend more easily because of the spiraling grain. The bending allows trees to become more effective at discarding excessive snow from their branches and more resistant to breakage from heavy wind.

This qualitative analysis, however, does not tell us how large the angle of the spiraling is. Stress analysis is performed to estimate that angle. The structure of the paper is as follows. In the next section, we analyze the stresses in an anisotropic cylinder that models the tree's trunk. This stress analysis considers the structure under an axial loading and bending moment. The stresses are computed as a function of the grain angle. The objective is to determine the influence of the grain angle on the strength of the structure. To estimate the strength, the Tsai-Hill failure criterion is used.

The problem considered is an example of the inverse optimization problem (Cherkaev, E. and Cherkaev, A. 1999) that arises in evolution biology. Studying morphology like bones or trunks which are critical for the survival of a species, we may postulate that they are optimally adapted to the environment. Trees' trunks should stay unbroken and be able to sustain extreme wind loads applied from all directions. If a natural design becomes more complex, there must be a reason for this. We treat the evolutionary development of the species as the minimizing sequence of an optimization problem with an unknown objective.

Notice that the optimization problems in engineering and in biology are mutually reciprocal. The biological structure is known, but it is not clear in what sense the structure is optimal. By contrast, the goal of the engineering is the minimization of a given functional that is not the subject of a search; the problem is to find an unknown optimal structure. This observation reflects the principal difference between biology which seeks an answer to the question of why bio-materials and the biomimetics of living organisms are the way they are and engineering which wants to know how to make an optimal structure.

2 Analysis

Before solving for the stress fields of this structure, we give a brief overview of equations required for the computation. Consider an infinite cylinder of radius R, filled with an orthotropic linear elastic material with compliance $\mathbf{S}$, and loaded by bending moment M and axial load P. We want to compute the stresses and strength of the cylinder, and to trace their dependence on the angle of twist of the anisotropic material. We assume that the stresses inside the cylinder satisfy equations of linear elasticity:

$$0 = \nabla \cdot \boldsymbol{\sigma} \,,$$

$$\boldsymbol{\sigma} = \boldsymbol{\sigma}^T \,,$$

$$\boldsymbol{\varepsilon} = \mathbf{S} \cdot \boldsymbol{\sigma} \,,$$

$$\boldsymbol{\varepsilon} = \frac{1}{2}\left[\nabla \mathbf{u} + (\nabla \mathbf{u})^T\right] .$$

Consider a differential element of the structure. The compliance of an orthotropic material can be expressed in terms of the engineering elastic parameters. In the coordinates that coincide with the principal axes of the anisotropy tensor (direction of the grain), Hooke's law takes the form

$$\varepsilon^*_{ij} = S^*_{ijkl}\sigma^*_{ij} \,,$$

where ε^*_{ij} are strain components, including both normal and shear, σ^*_{ij} are stress components, including both normal and shear, and S^*_{ijkl} is the compliance matrix. In matrix form,

$$\begin{Bmatrix} \epsilon^*_{11} \\ \epsilon^*_{22} \\ \epsilon^*_{33} \\ \epsilon^*_{23} \\ \epsilon^*_{13} \\ \epsilon^*_{12} \end{Bmatrix} = \begin{bmatrix} \frac{1}{E_{11}} & -\frac{\nu_{21}}{E_{22}} & -\frac{\nu_{31}}{E_{33}} & 0 & 0 & 0 \\ -\frac{nu_{21}}{E_{11}} & \frac{1}{E_{22}} & \frac{\nu_{32}}{E_{33}} & 0 & 0 & 0 \\ -\frac{nu_{31}}{E_{11}} & \frac{\nu_{23}}{E_{22}} & \frac{1}{E_{33}} & 0 & 0 & 0 \\ 0 & 0 & 0 & \frac{1}{G_{23}} & 0 & 0 \\ 0 & 0 & 0 & 0 & \frac{1}{G_{13}} & 0 \\ 0 & 0 & 0 & 0 & 0 & \frac{1}{G_{12}} \end{bmatrix} \begin{Bmatrix} \sigma^*_{11} \\ \sigma^*_{22} \\ \sigma^*_{33} \\ \sigma^*_{23} \\ \sigma^*_{13} \\ \sigma^*_{12} \end{Bmatrix} . \tag{1}$$

The subscript 1 represents the radial direction. Directions perpendicular and parallel to the grain are denoted by subscripts 2 and 3, respectively (see Fig. 2).

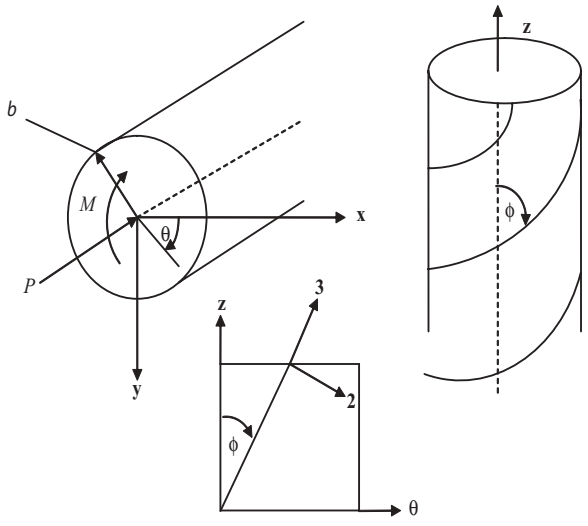

Fig. 2 Schematic of the tree trunk

2.1 Transformation of $\mathbf{S}^*$

The structure possesses cylindrical anisotropy. Hence, the analysis is conducted in cylindrical coordinates. We need to compute the components of (1) in the cylindrical system. The main coordinate axes of the compliance $\mathbf{S}^*$ are directed as follows:

$$\mathbf{e}_r = \mathbf{e}_1 \,,$$

$$\mathbf{e}_\theta = \cos\phi\mathbf{e}_2 + \sin\phi\mathbf{e}_3 \,,$$

$$\mathbf{e}_z = -\sin\phi\mathbf{e}_2 + \cos\phi\mathbf{e}_3 \,.$$

The new matrix can be written as

$$\mathbf{S} = \left(\mathbf{K}^{-1}\right)^T \mathbf{S}^*\mathbf{K}^{-1} \,,$$

where $\mathbf{S}$ is the compliance matrix in cylindrical coordinates and $\mathbf{K}$ is a rotation matrix. It has a block form (Ting 1996):

$$\mathbf{K} = \begin{bmatrix} \mathbf{K}_1 & 2\mathbf{K}_2 \\ \mathbf{K}_3 & \mathbf{K}_4 \end{bmatrix} \,, \tag{2}$$

where

$$\mathbf{K}_1 = \begin{bmatrix} \Omega_{11}^2 & \Omega_{12}^2 & \Omega_{13}^2 \\ \Omega_{21}^2 & \Omega_{22}^2 & \Omega_{23}^2 \\ \Omega_{31}^2 & \Omega_{32}^2 & \Omega_{33}^2 \end{bmatrix} \,,$$

$$\mathbf{K}_2 = \begin{bmatrix} \Omega_{12}\Omega_{13} & \Omega_{13}\Omega_{11} & \Omega_{11}\Omega_{12} \\ \Omega_{22}\Omega_{23} & \Omega_{23}\Omega_{21} & \Omega_{21}\Omega_{22} \\ \Omega_{32}\Omega_{33} & \Omega_{33}\Omega_{31} & \Omega_{31}\Omega_{32} \end{bmatrix} \,,$$

$$\mathbf{K}_3 = \begin{bmatrix} \Omega_{21}\Omega_{31} & \Omega_{22}\Omega_{32} & \Omega_{23}\Omega_{33} \\ \Omega_{31}\Omega_{11} & \Omega_{32}\Omega_{12} & \Omega_{33}\Omega_{13} \\ \Omega_{11}\Omega_{21} & \Omega_{12}\Omega_{22} & \Omega_{13}\Omega_{23} \end{bmatrix} \,,$$

$$\mathbf{K}_4 = \begin{bmatrix} L_1 & L_2 & L_3 \\ L_4 & L_5 & L_6 \\ L_7 & L_8 & L_9 \end{bmatrix} \,,$$

and

$$\mathbf{L}_1 = \Omega_{22}\Omega_{33} + \Omega_{23}\Omega_{32} \,,$$

$$\mathbf{L}_2 = \Omega_{23}\Omega_{31} + \Omega_{21}\Omega_{33} \,,$$

$$\mathbf{L}_3 = \Omega_{21}\Omega_{32} + \Omega_{22}\Omega_{31} \,,$$

$$\mathbf{L}_4 = \Omega_{32}\Omega_{13} + \Omega_{33}\Omega_{12} \,,$$

$$\mathbf{L}_5 = \Omega_{33}\Omega_{11} + \Omega_{31}\Omega_{13} \,,$$

$$\mathbf{L}_6 = \Omega_{31}\Omega_{12} + \Omega_{32}\Omega_{11} \,,$$

$$\mathbf{L}_7 = \Omega_{12}\Omega_{23} + \Omega_{13}\Omega_{22} \,,$$

$$\mathbf{L}_8 = \Omega_{13}\Omega_{21} + \Omega_{11}\Omega_{23} \,,$$

$$\mathbf{L}_9 = \Omega_{11}\Omega_{22} + \Omega_{12}\Omega_{21} \,.$$

Here, Ω_{ij} are the elements of the matrix

$$\boldsymbol{\Omega} = \begin{bmatrix} 1 & 0 & 0 \\ 0 & \cos\phi & \sin\phi \\ 0 & -\sin\phi & \cos\phi \end{bmatrix} \,. \tag{3}$$

After the transformation, the matrix $\mathbf{S}$ takes the following form:

$$\mathbf{S} = \begin{bmatrix} a_{11} & a_{12} & a_{13} & a_{14} & 0 & 0 \\ a_{21} & a_{22} & a_{23} & a_{24} & 0 & 0 \\ a_{31} & a_{32} & a_{33} & a_{34} & 0 & 0 \\ a_{41} & a_{42} & a_{43} & a_{44} & 0 & 0 \\ 0 & 0 & 0 & 0 & a_{55} & a_{56} \\ 0 & 0 & 0 & 0 & a_{65} & a_{66} \end{bmatrix} \,,$$

where a_{ij} are the non-zero rotated elements that are determined from (2) and (3). The stresses and strains are transformed as follows:

$$\boldsymbol{\sigma} = \mathbf{K}\boldsymbol{\sigma}^* \text{ and } \boldsymbol{\varepsilon} = \left(\mathbf{K}^{-1}\right)^T \boldsymbol{\varepsilon}^* \,,$$

where $\boldsymbol{\sigma}$ and $\boldsymbol{\varepsilon}$ are the stress and strain in cylindrical coordinates.

Below, the stresses are analyzed for two loading cases: axial loading and bending. Due to the linearity of the model, the stresses are the sum of the results from these two loadings.

2.2 Stress functions

In this analysis, the body force is neglected; the cylinder is loaded from its ends. The cylindrical coordinate system as shown previously in Fig. 2 is used. It is independent of z. Thus, the equilibrium equations in cylindrical coordinates become

$$\frac{\partial\sigma_r}{\partial r} + \frac{1}{r}\frac{\partial\tau_{r\theta}}{\partial\theta} + \frac{\sigma_r - \sigma_\theta}{r} = 0 \,,$$

$$\frac{\partial\tau_{r\theta}}{\partial r} + \frac{1}{r}\frac{\partial\sigma_\theta}{\partial\theta} + \frac{2\tau_{r\theta}}{r} = 0 \,,$$

$$\frac{\partial\tau_{rz}}{\partial r} + \frac{1}{r}\frac{\partial\tau_{\theta z}}{\partial\theta} + \frac{\tau_{rz}}{r} = 0 \,,$$

and

$$\sigma_z = \frac{1}{a_{33}} \left(D - a_{13}\sigma_r - a_{23}\sigma_\theta - a_{34}\tau_{\theta z} - a_{35}\tau_{rz} \; - a_{36}\tau_{r\theta} \right) , \tag{4}$$

where $D = Br\sin\theta + C$ (see Lekhnitskii (1981)). These four equations link six components of the stress tensor $\sigma_r, \sigma_\theta, \sigma_z, \tau_{\theta z}, \tau_{rz}$, and $\tau_{r\theta}$ (see Fig. 3). The other coefficients, B and C, are constants that result from the boundary conditions. To solve for the stress fields satisfying the equilibrium equations, two stress functions, $\Phi(r,\theta)$ and $\Psi(r,\theta)$, are introduced, as is common in the theory of elasticity (see for example Lekhnitskii (1981)). The stress components are expressed through Φ and Ψ as

$$\sigma_r = \frac{1}{r}\frac{\partial \Phi}{\partial r} + \frac{1}{r^2}\frac{\partial^2 \Phi}{\partial \theta^2} ,$$

$$\tau_{r\theta} = -\frac{\partial^2}{\partial r \partial \theta}\left(\frac{\Phi}{r}\right) , \qquad \sigma_\theta = \frac{\partial^2 \Phi}{\partial r^2} , \tag{5}$$

$$\tau_{\theta z} = -\frac{\partial \Psi}{\partial r} , \qquad \tau_{rz} = \frac{1}{r}\frac{\partial \Psi}{\partial \theta} .$$

Notice that σ_z is expressed through the other components by (4). According to Lekhnitskii (1981), the stress functions must satisfy the following equations:

$$L_4'\Phi + L_3'\Psi = \frac{2}{a_{33}}\left(a_{13} - a_{33}\right)\frac{B\sin\theta}{r} , \tag{6}$$

$$L_3''\Phi + L_2'\Psi = \frac{2a_{34}B\sin\theta}{a_{33}} + \frac{a_{34}C}{r} - 2\xi , \tag{7}$$

where L_4', L_3', L_3'', and L_2' are differential operators of the fourth, third, and second orders, respectively:

$$L_4' = \beta_{22}\frac{\partial^4}{\partial r^4} + \left(2\beta_{12} + \beta_{66}\right)\frac{1}{r^2}\frac{\partial^4}{\partial r^2 \partial \theta^2} + \beta_{11}\frac{1}{r^4}\frac{\partial^4}{\partial \theta^4} +$$

$$2\beta_{22}\frac{1}{r}\frac{\partial^3}{\partial r^3} - \left(2\beta_{12} + \beta_{66}\right)\frac{1}{r^3}\frac{\partial^3}{\partial r \partial \theta^2} - \beta_{11}\frac{1}{r^2}\frac{\partial^2}{\partial r^2} +$$

$$\left(2\beta_{11} + 2\beta_{12} + \beta_{66}\right)\frac{1}{r^4}\frac{\partial^2}{\partial \theta^2} + \beta_{11}\frac{1}{r^3}\frac{\partial}{\partial r} ,$$

$$L_3' = -\beta_{24}\frac{\partial^3}{\partial r^3} - \left(\beta_{14} + \beta_{56}\right)\frac{1}{r^2}\frac{\partial^3}{\partial r \partial \theta^2} +$$

$$\left(\beta_{14} - 2\beta_{24}\right)\frac{1}{r}\frac{\partial^2}{\partial r^2}$$

$$L_3'' = -\beta_{24}\frac{1}{r}\frac{\partial^3}{\partial r^3} - \left(\beta_{14} + \beta_{56}\right)\frac{1}{r^2}\frac{\partial^3}{\partial r \partial \theta^2} -$$

$$\left(\beta_{14} + \beta_{24}\right)\frac{1}{r}\frac{\partial^2}{\partial r^2} + \left(\beta_{14} + \beta_{56}\right)\frac{1}{r^3}\frac{\partial^2}{\partial \theta^2} ,$$

$$L_2' = \beta_{44}\frac{\partial^2}{\partial r^2} + \beta_{55}\frac{1}{r^2}\frac{\partial^2}{\partial \theta^2} + \beta_{44}\frac{1}{r}\frac{\partial}{\partial r} ,$$

and

$$\beta_{ij} = a_{ij} - \frac{a_{i3}a_{j3}}{a_{33}}$$

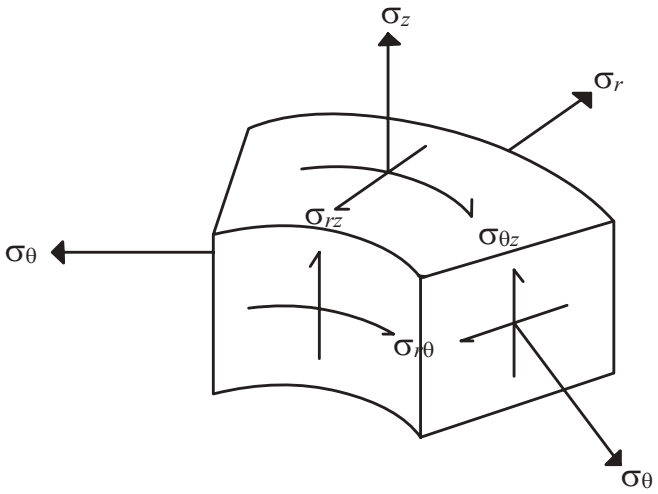

Fig. 3 Stress components in cylindrical coordinates

is the reducing strain coefficient. Derivations of these differential operators and their explicit forms are given in Lekhnitskii (1981).

2.3 Stresses due to axial loading

In the case of axial loading, the stress functions and the components of stress depend only on r. Thus, the solutions to (6) and (7) are sought in the form

$$\Phi = f(r) \quad \Psi = g(r) . \tag{8}$$

Therefore, the parameters on the right-hand sides of (6) and (7) are zero. Substituting (8) into (6) and (7), the following system of differential equations is obtained:

$$0 = \beta_{22}f^{IV} + \frac{2\beta_{22}}{r}f''' -$$

$$\frac{\beta_{11}}{r^2}f'' + \frac{\beta_{11}}{r^3}f' - \beta_{24}g''' + \frac{\left(\beta_{14} - 2\beta_{24}\right)}{r}g'' , \tag{9}$$

$$\frac{a_{34}C}{r} - 2\xi = \beta_{24}f''' + \frac{\left(\beta_{14} + \beta_{56}\right)}{r^2}f' + \beta_{44}g'' + \frac{\beta_{44}}{r^2}g' . \tag{10}$$

We look for the solutions to the homogeneous part of (9) and (10) in the form

$$f_h = Fr^\alpha \quad g_h = Gr^{\alpha-1} . \tag{11}$$

The subscript h denotes a homogeneous solution. By substituting (11) into (9) and (10), r is eliminated, and we obtain the system

$$\underbrace{\begin{bmatrix} H_1(\alpha) & H_2(\alpha) \\ H_3(\alpha) & H_4(\alpha) \end{bmatrix}}_{\mathbf{H}} \begin{bmatrix} F \\ G \end{bmatrix} = \begin{bmatrix} 0 \\ 0 \end{bmatrix} . \tag{12}$$

The homogeneous system has nontrivial solutions for F and G only if $\det(\mathbf{H}) = 0$. In solving this relation, we obtain six parameters for $\alpha : 0, 0, 1, 2, \alpha_5$, and α_6. The stress functions can now be expressed as

$$\Phi = \left(m_1 + m_2 \ln r + m_3 r + m_4 r^2 + m_5 r^{\alpha_5} + m_6 r^{\alpha_6}\right) + \Phi_p \,, \tag{13}$$

$$\Psi = \left(p_1 r^{-1} + p_2 r^{-1} \ln r + p_3 + p_4 r + p_5 r^{\alpha_5 - 1} + p_6 r^{\alpha_6 - 1}\right) + \Psi_p \,, \tag{14}$$

where $m_1 ... m_6$, $p_1 ... p_6$ are constants. Φ_p and Ψ_p are the particular solutions $\Phi_p = a_1 r^3$ and $\Psi_p = b_1 r^2 + c_1 r$.

Considering the condition at point $r = 0$, one can see that $m_2 = m_3 = m_4 = p_1 = p_2 = p_4 = 0$ in order to avoid the singularity at this location. Moreover, any value of α_i that has a negative sign is discarded because stresses have to be finite. In this case, either α_5 or α_6 has a negative value. Let us assign these values to α_5, so that $m_5 = p_5 = 0$. The stress functions now become

$$\Phi = m_6 r^{\alpha_6} + \Phi_p \,, \quad \Psi = p_6 r^{\alpha_6 - 1} + \Psi_p \,.$$

The unknown constants are determined from the boundary conditions:

$$\sigma_r = \tau_{r\theta} = \tau_{\theta z} = \tau_{rz} = 0 \text{ at } r = b \,. \tag{15}$$

Utilizing (15), we have two equations with two unknowns. The constants in the particular solutions are determined from the end conditions:

$$\int_0^b \sigma_z r \, \mathrm{d}r = \frac{P}{\pi b^2} \,, \quad \int_0^b \tau_{\theta z} r^2 \, \mathrm{d}r = 0 \,,$$

where P is the axial loading and b is the radius of the cylinder. Once all the constants are determined, stress components can then be evaluated according to (5). Because of the spiral anisotropy, the axial loading causes the cylinder to twist. The displacements are not computed in this analysis, since the main objective is to determine the stresses.

2.4 Stresses due to bending

Let us analyze the case in which the structure is in pure bending. A bending moment M is applied at each end (Fig. 2). The analysis still follows the same procedures as in the axial loading case, but with different stress functions:

$$\Phi = f(r) \sin\theta \quad \Psi = g(r) \sin\theta \,.$$

In the pure bending case, C and ξ in (6) and (7) are zero. By substituting the above stress functions into (6) and (7), the following system of differential equations is obtained:

$$\frac{2\left(a_{13} - a_{33}\right) B}{a_{33} r} =$$

$$\beta_{22} f^{IV} - \frac{(2\beta_{12} + \beta_{66})}{r^2} f'' + \frac{\beta_{11}}{r^4} f + \frac{2\beta_{22}}{r} +$$

$$\frac{(2\beta_{12} + \beta_{66})}{r^3} f' - \frac{\beta_{11}}{r^2} f'' - \frac{(2\beta_{11} + 2\beta_{12} + \beta_{66})}{r^4} f +$$

$$\frac{\beta_{11}}{r^3} f' - \beta_{24} g''' + \frac{(\beta_{14} + \beta_{56})}{r^2} g + \frac{(\beta_{14} - 2\beta_{24})}{r} g'' \,, \tag{16}$$

$$\frac{2 a_{34} B}{a_{33}} = -\beta_{24} f''' + \frac{(\beta_{14} + \beta_{56})}{r^2} f' - \frac{(\beta_{14} + \beta_{24})}{r} f'' -$$

$$\frac{(\beta_{14} + \beta_{56})}{r^3} f + \beta_{44} g'' + \frac{\beta_{55}}{r^2} g + \frac{\beta_{55}}{r^2} g' \,. \tag{17}$$

Similarly to the axial loading case, the solutions to the homogeneous part of (16) and (17) assume the forms of (11), and α is solved as described in the axial loading case by using (12). Solving (12) yields six values, 1, 1, α_3, α_3, α_4, α_5, and α_6. Their expressions are shown in Appendix. The stress functions can now be expressed as

$$\Phi = (m_1 r + m_2 r \ln r + m_3 r^{\alpha_3} + m_4 r^{\alpha_4} + m_5 r^{\alpha_5} + m_6 r^{\alpha_6}) \sin\theta + \Phi_p \,,$$

$$\Psi = \left(p_1 + p_2 \ln r + p_3 r^{\alpha_3 - 1} + p_4 r^{\alpha_4 - 1} + p_5 r^{\alpha_5 - 1} + p_6 r^{\alpha_6 - 1}\right) \sin\theta + \Psi_p \,,$$

where $\Phi_p = a_1 r^3 \sin\theta$ and $\Psi_p = b_1 r^2 \sin\theta$. Once again, by setting the condition at $r = 0$, one can see that m_2 and p_2 are zero, and, as in the axial loading case, any value of α_i that has a negative sign is omitted. Now, the stress functions become

$$\Phi = (m_3 r^{\alpha_3} + m_4 r^{\alpha_4}) \sin\theta + \Phi_p \,,$$

$$\Psi = \left(p_3 r^{\alpha_3 - 1} + p_4 r^{\alpha_4 - 1}\right) \sin\theta + \Psi_p \,.$$

The unknown constants m_3, m_4, p_3, and p_4 are determined from the boundary conditions:

$$\sigma_r = \tau_{r\theta} = \tau_{\theta z} = \tau_{rz} = 0 \text{ at } r = b \,. \tag{18}$$

By utilizing (18), a system of four equations and four unknowns is obtained. The constants in the particular solutions are determined from the end conditions:

$$\int_0^{2\pi} \int_0^b \sigma_z r^2 \sin\theta \, \mathrm{d}r \, \mathrm{d}\theta = M \,,$$

$$\int_0^{2\pi} \int_0^b \sigma_z r^2 \cos\theta \, \mathrm{d}r \, \mathrm{d}\theta = 0 \,.$$

Finally, stress components can then be evaluated according to (5). This computation was carried out by using Maple V. This analysis enables us to compute stresses in an anisotropic elastic cylinder with rotated axes of anisotropy. Although the calculations are analytic, the resulting formulas (obtained by Maple V) are bulky and we do not display them here.

2.5 Failure criteria

Due to the nature of the anisotropy, the conventional maximum strength criterion for isotropic materials gives a poor prediction of failure (Swanson 1997). For wood, we use the Tsai–Hill failure criterion:

$$\left(\frac{\sigma_1}{\sigma_{1u}}\right)^2 + \left(\frac{\sigma_2}{\sigma_{2u}}\right)^2 - \frac{\sigma_1\sigma_2}{\sigma_{1u}^2} + \left(\frac{\tau_{12}}{\tau_{12u}}\right)^2 < 1\,. \tag{19}$$

When the left-hand side of (19) is greater than or equal to 1, failure is predicted. No distinction is made between compressive and tensile stresses.

Another criterion that is often used for wood structure is Hankison's formula (Gedney 1986):

$$\sigma_u = \frac{\sigma_{1u}\sigma_{2u}}{\sigma_{1u}\sin^2\phi + \sigma_{2u}\cos^2\phi}\,.$$

Hankinson's formula approximates the ultimate axial strength as a function of the grain angle.

3 Analysis of the Ponderosa pine

Based on the pure mechanical model presented in the previous section, the stresses were determined for the Ponderosa pine. First, the stresses were computed for the case of axial loading and then for the case of a bending moment. The computation of stresses demonstrates whether spiraling is related to the elastic properties of the tree. If nature has already optimized the structure of living organisms, one expects the structure of the tree to be optimized for the environment surrounding it. For instance, the structure of the tree should be in the configurations that maximize its strength to support the weight of branches, leaves, snow, and also resistance to wind.

Table 1 Elastic moduli of Ponderosa pine with 12% moisture content, 10^6 psi

E_1	E_2	E_3	G_{12}	G_{13}	G_{23}
0.1236	0.0743	1.423	0.00994	0.1035	0.0978

3.1 Setting of the parameters

We assumed that the trunk of the Ponderosa pine was cylindrical with radius $r = 10$ in. In addition, the axial loading was only a result of the weight and has the magnitude $P = 1500$ lb. The bending moment was approximated to be 10 000 lb in. from the wind force. All the parameters were approximated in English units in order to apply directly to the data that have been obtained for the Ponderosa pine. Table 1 shows the properties of the Ponderosa pine (Bodig and Jayne 1996). The material strengths were (The Forest Products Laboratory 1955) $\sigma_{33t} = 6300$ psi, $\sigma_{33c} = -5270$ psi, $\sigma_{22t} = 400$ psi, $\sigma_{22c} = -740$ psi, and $\tau_{23ul} = 1160$ psi.

By utilizing this information, the calculation of stresses was performed. In this case, if the spiral angle is less than 21.2°, some α's in (13) and (14) become negative. This leads to a singularity at the center of the trunk at which $r = 0$. As a result, we only looked at values of the grain angle ϕ varying from 21.2° to 90°. By applying (19), we could predict when the structure fails.

3.2 Results

Figure 4 shows the total stresses resulting from bending and axial loading. Here, we looked at the stresses and the maximal grain angle of the Ponderosa pine by using data and criteria given in Sect. 3.1 and Sect. 2.5. In addition, stresses were only investigated on the surface at $\theta = 90°$ and $\theta = -90°$ because maximum compressive and tensile stresses were expected at these locations. Only the plots of the stress fields are illustrated due to the size of the stress equations. Since P and M were chosen arbitrarily, it is interesting to see how the failure prediction varies if P or M changes. It is appropriate to vary M since the speed of the wind varies more than the weight on top of the tree. The grain angle and the Tsai–Hill minimum failure values are shown in Fig. 5.

As the magnitude of the bending moment increases, the maximal grain angle becomes smaller in order to reduce the bending stress. The maximal grain angle is approximately 37° (Fig. 5). At this grain angle, the Ponderosa pine fails when the magnitude of the bending moment increases to 800 kip in. Naturally, trees are uprooted when the wind load is high. The stresses produced by the wind load in nature are not typically high enough to exceed the strength of this tree. The ultimate strength of the Ponderosa pine is shown in Fig. 6 using Hankinson's formula and the Tsai–Hill failure criterion.

4 Structural optimization

In the beginning, we mentioned that spiraling allows the fluid to be transferred throughout the whole tree even

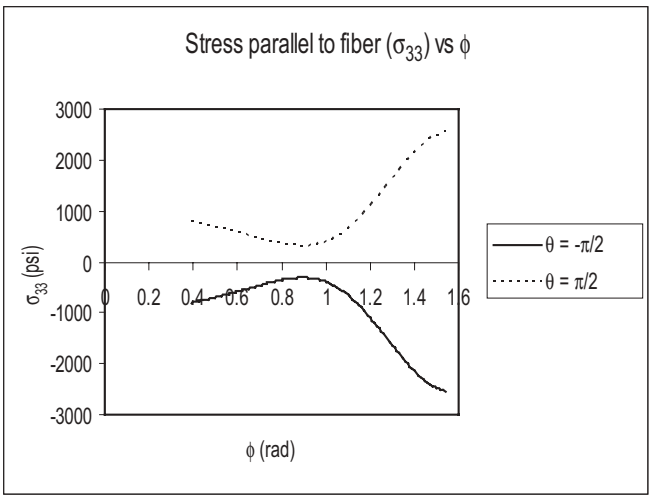

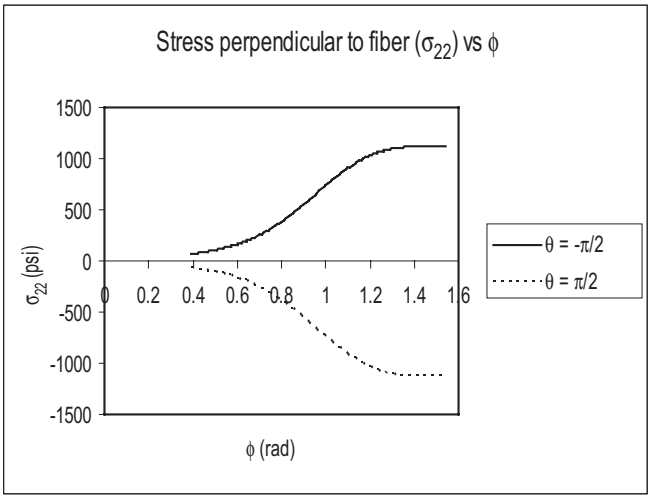

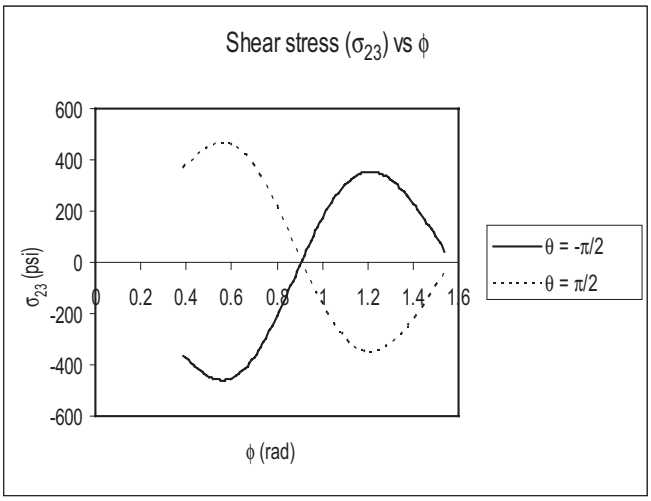

Fig. 4 Total stresses on the surface of the tree

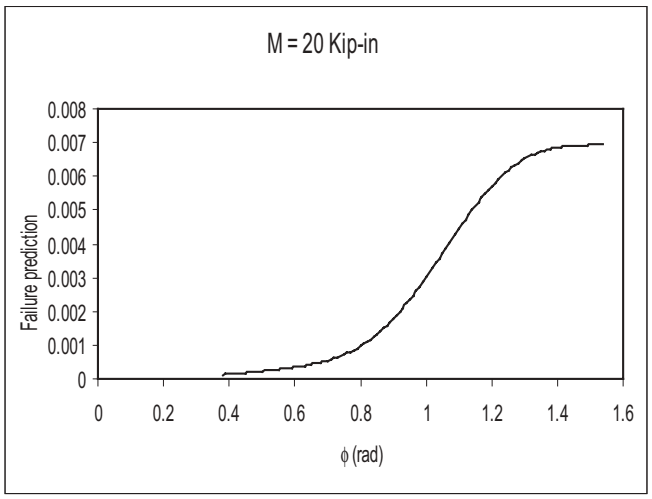

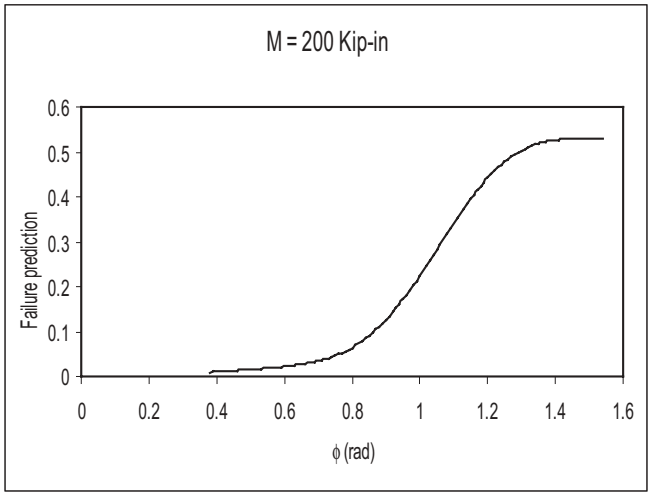

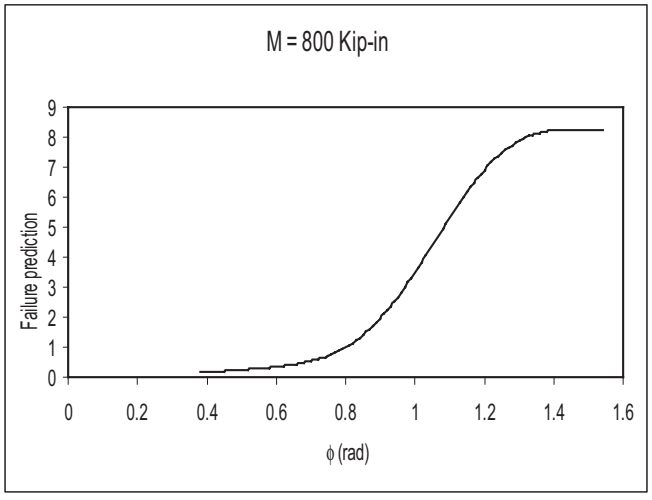

Fig. 5 Failure prediction using Tsai–Hill criterion at $\theta = \frac{\pi}{2}$

if the roots on one side have died. However, the presence of spiraling also causes the tree to become less stiff. Hence, we need to determine the maximum grain angle that does not affect the strength of the tree significantly.

Having obtained the results of the failure predictions, one may use them to gain the benefits of the biomimetics of these trees. From Fig. 5, we can see that the curves from these plots have the same shape but with different magnitudes. These curves show that there is a sharp in-

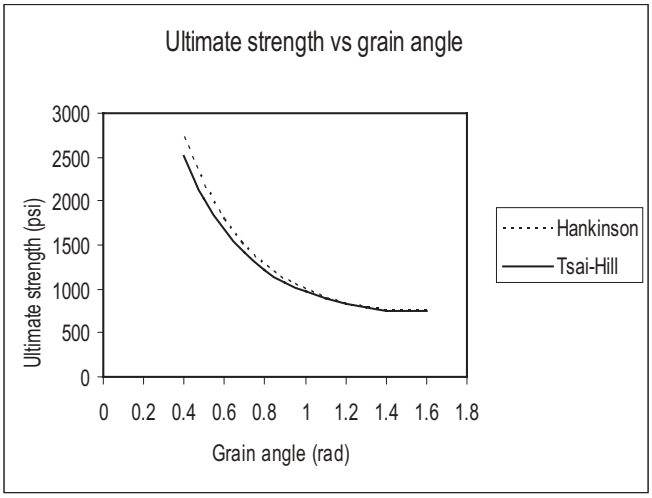

Fig. 6 Ultimate strength of Ponderosa pine at various spiral angles

crease in magnitude beyond 37°. From this observation, one could set up the problem of finding the maximum angle as a problem of optimization with constraints as follows:

Maximize the angle ϕ $(0 \leq \phi \leq \frac{\pi}{2})$ subject to the conditions

1. The failure criterion (19) is satisfied
2. Parameters of materials and loadings are as described in Sect. 3.1
3. The angle ϕ is within the range preceding the point where the sharp increase of the slope in Fig. 5 takes place.

5 Discussion and conclusions

From this analysis, one cannot fully explain the relationship between the spiral twist and the mechanical properties of the tree; it is more reasonable to assume that the spiraling has to do with the fluid transportation that we mentioned in the introduction. Instead, it might be more appropriate to ask how big the angle can be in order for the tree to remain strong. Excessive spiraling not only reduces the stiffness of the tree but also weakens the strength of the tree. Hence, there ought to be a limiting point on how much the stiffness can be reduced in order for a tree to stand up straight. Its chance against breaking would increase if it does not bend much.

The result from Fig. 5 shows that the failure prediction value increases slowly to about 37°, and then the slope increases dramatically beyond this point. The tree strength is not sacrificed considerably as long as the grain angle remains below 37°. The grain angle of the Ponderosa tree obtained by using theory of anisotropic elasticity is slightly different from the angle measured in Fig. 7. However, this was expected since many assumptions were made during the analysis. The permitted interval according to this analysis is between 21.2° and 37°.

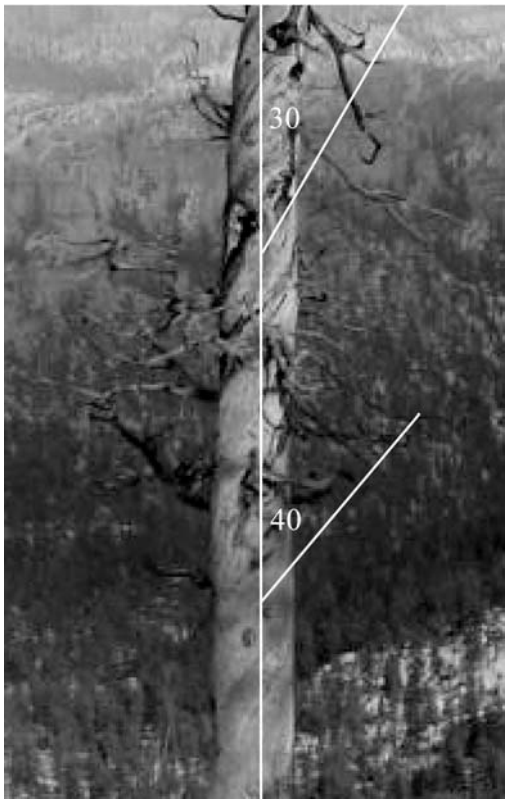

Fig. 7 Angle measurements at the lower and upper portions of the trunk

Another observation that was made was the differences between the lower and the upper portion of the tree (Fig. 7). The grain angle is a little bigger toward the bottom. When the tree is small, it requires more distribution of fluid to ensure proper growth. Having the fiber spiral at a bigger angle allows the tree to receive more fluid along its circumference. As the tree grows taller, the angle becomes smaller, which allows the fluid to be transported to the higher portion faster by reducing the coverage area. This could be another reason why the grain angle varies in this way. Details about fluid transportation are not discussed here since it is beyond the scope of this analysis.

We did not consider the cracking of the trunk in this analysis. Nevertheless, it may be an important factor. Looking at the elastic constants of this tree, one finds that E_2 is approximately 5% of E_3, which is almost the value it should be if there is a crack. With this in mind, Leonid Slepyan (via private communication) has pointed out that, as the crack wiggles around the tree, it is less prone to fracture than when the crack is vertically straight.

Due to a lack of information and actual data on the average wind load and the load that can uproot the Ponderosa tree, it is not possible to give a solid conclusion regarding relationships between the magnitude of the twist and the elastic properties of trees. In addition, the results presented in this analysis only reflect the properties of the Ponderosa pine.

Our analysis shows that the problem of adaptation of a tree trunk can be viewed as a problem of constrained minimization. The spirals in the grain are developed for a non-mechanical reason (transport of water to branches) and the strength analysis provides a constraint that limits the angle of these spirals. Namely, we observe that the strength is practically the same for angles that do not surpass the critical value, and this critical value is what we see in nature. In short, a structure can be more flexible by having the fibers spiral along its circumference. However, depending on the elastic properties of the material, the angle of the spiral can vary.

Acknowledgements We are indebted to many people who encouraged us and advised us on different aspects of the modeling and analysis. Their general comments and suggestions were sound and worthwhile. In particular, we mention the help from Tim Folias, Stephen Swanson, Leonid Slepyan, Steve Cowin, Jack H.T. Chang, and Natalya Kizilova. A special thanks goes to Roderic Lakes, who offered numerous suggestions on the first draft. The problem was presented for discussion on our website http://www.math.utah.edu/ cherk, and we enjoyed numerous comments from colleagues, to whom we are thankful. The work was sponsored by National Science Foundation (NSF Grant No. DMS- 0072717).

References

Bodig, J.; Jayne, B.A. 1996: *Mechanics of Woods and Wood Composites*. New York: Van Nostrand Reinhold

Cherkaev, E.; Cherkaev, A. 1999: Structural optimization and biological "designs". In: *Solid Mechanics and its Applications. v. 69: Synthesis in Bio Solid Mechanics*. Bendsoe, M.; Pedersen, P. (eds.) Dordrecht: Kluwer Academic Press, pp. 247–264

The Forest Products Laboratory 1955: *Wood Handbook, No. 19*. Washington, D.C.: U.S. Department of Agriculture, 76

Gedney, L. 1986: Alaska Science Forum, Art. 783

Kubler, H. 1991: Trees **5**, 125–135

Lekhnitskii, S.G. 1981: *Theory of Elasticity of an Anisotropic Body*. Moscow: MIR Publishers

Swanson, S.R. 1997: *Introduction to Design and Analysis with Advanced Composite Materials*. New Jersey: Prentice-Hall

Ting, T.C.T. 1996: *Anisotropic Elasticity: Theory and Applications*. New York: Oxford University Press